FERMILAB-CONF-07-387-TD

QUENCH PERFORMANCE OF Nb_3Sn COS-THETA COILS MADE OF 108/127 RRP STRANDS

A.V. Zlobin[1], G. Ambrosio[1], N. Andreev[1], E. Barzi[1], R. Bossert[1], R. Carcagno[1], V.S. Kashikhin[1], V.V. Kashikhin[1], M.J. Lamm[1], F. Nobrega[1], I. Novitski[1], D. Orris[1], Yu. Pischalnikov[1], D. Shpakov[1], C. Sylvester[1], M. Tartaglia[1], J.C. Tompkins[1], D. Turrioni[1], R. Yamada[1], A. Yuan[1].

[1]Fermi National Accelerator Laboratory
Batavia, Illinois, 60506, USA

ABSTRACT

A series of 1-m long Nb_3Sn dipole models has been built at Fermilab in an attempt to refine the wind-and-react technology for Nb_3Sn accelerator magnets. Three models made with Powder-in-Tube Nb_3Sn strand reached their design field of 10 T demonstrating a good reproducibility of magnet quench performance and field quality. Recently a new dipole "mirror" model based on Nb_3Sn coil made of improved Restack Rod Process strand was constructed and tested reaching the maximum field above 11 T. This paper describes the parameters of the RRP strand and cable used as well as the design, fabrication and test results of this magnet.

KEYWORDS: Dipole magnet, cos-theta coil, cable, strand, Nb_3Sn, quench performance.

INTRODUCTION

Fermilab is developing accelerator magnets based on Nb_3Sn shell-type coils and the wind-and-react technology. Six 1-m long Nb_3Sn dipole models, three based on Modified Jelly Roll (MJR) and three based on Powder-in-Tube (PIT) 1 mm strand, have been built and tested. The quench performances of the MJR models, which used high-Jc strand with large sub-element size and low RRR, was limited by flux jump instabilities in superconductor [1]. The PIT models with lower Jc, smaller filament size and high RRR reached their design field of 10 T demonstrating a good reproducibility of magnet quench performance [2]. To further advance the field in this magnet design, the high performance Nb_3Sn strand produced by Oxford Superconducting Technology (OST) using the Restack Rod Process (RRP) [3] has been chosen. To improve the strand stability in the current and field ranges expected in the magnet models, a new RRP strand design with increased number of sub-elements (108 subelements in the 127 restack array) was developed by OST, which resulted in a smaller filament size.

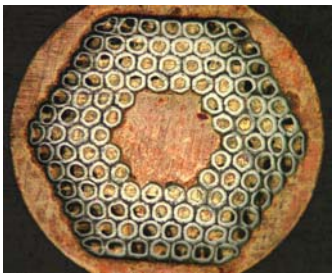

FIGURE 1. 108/127 RRP strand.

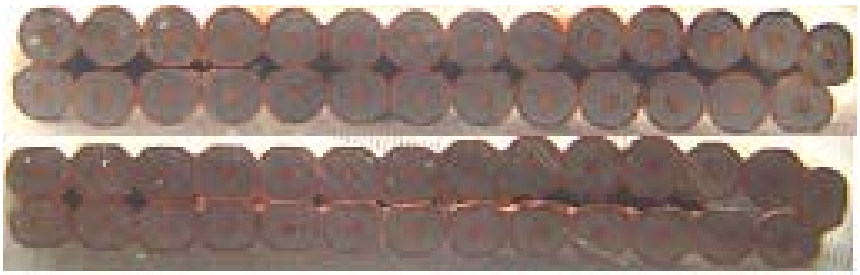

FIGURE 2. 27-strand rectangular and keystone cables.

The performance of the 1.0 mm strand with 108/127 restack design was extensively studied using virgin and deformed strand samples. Rutherford-type cables made of this strand were also tested using a superconducting transformer and small racetrack coils [4]. Based on the positive results of strand and cable tests, two shell-type dipole coils were fabricated and one of them was tested using a magnetic mirror configuration. This paper presents the parameters of the 108/127 RRP strand and cables made of it, describes the dipole coil design and fabrication procedure, and reports the results of coil testing.

STRAND AND CABLE DESCRIPTION

The cross section of the RRP strand with 108/127 stacks is shown in Figure 1. The strand diameter is 1.0 mm, copper fraction is 49% and twist pitch is 12 mm. The 108/127 stack RRP strand uses sub-elements made of pure Nb mixed with discreet Nb-47%Ti filaments, which allows forming $(Nb,Ti)_3Sn$ with high critical current density and upper critical field. With these sub-elements the RRP strand provided nominal Jc of ~2400 A/mm^2 at 12 T and Cu-matrix RRR above 200 [5].

The 27-strand Rutherford-type cables with rectangular (RC) and keystoned (KS) cross sections with 1-mm RRP strand of 108/127 stack design have been fabricated at Fermilab using 42-strand cabling machine [6]. The more compacted KS cable was made using the low compaction RC cable after short annealing at 190^{o}C in air. The parameters of both cables are described in Table I, and the cable cross-sections are shown in Figure 2.

COIL DESIGN AND FABRICATION

Dipole models of the HFDA series developed and used at Fermilab for the Nb_3Sn accelerator magnet technology development are described in [7, 8]. Their design is based on a two-layer shell-type coil and a cold iron yoke. The magnet bore diameter is 43.5 mm.

TABLE I. Cable Parameters.

Cable ID	RC	KS
Average width, mm	13.95	14.24
Average thickness, mm	1.95	1.801
Keystone angle, degree	0	0.91
Average lay angle, degree	14.5	14.5
Packing factor, %	81	86

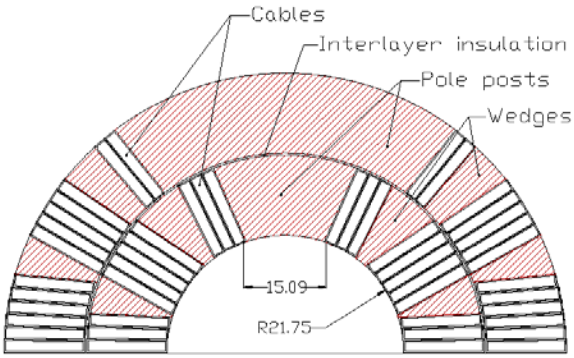

FIGURE 3. Half-coil cross section.

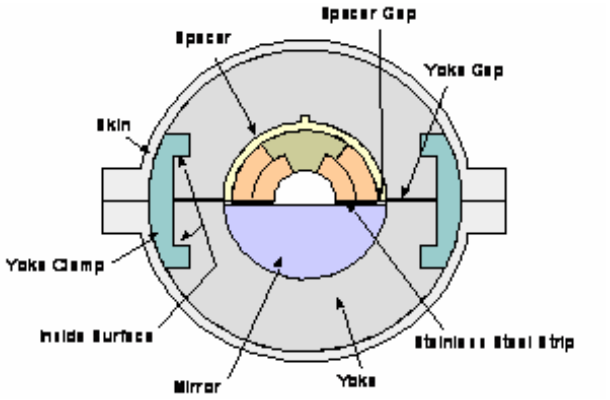

FIGURE 4. Dipole mirror mechanical structure.

The cross section of the dipole half-coil is shown in Figure 3. Each half-coil has 2 layers, with 16 turns and two spacers per quadrant in the inner layer, 21 turns and two spacers per quadrant in the outer layer, and separate pole blocks in each layer. Coil layers are separated with 0.4 mm thick inter-layer insulation. Coil ends have current blocks consistent with the coil straight section and separated by metallic spacers.

The coil was wound from a single piece of ~50 m long cable without an inter-layer splice. The cable insulation consisted of 0.125 mm thick and 12.5 mm wide ceramic tape, spiral wound over the cable with approximately 45% overlap. After winding of the inner layer, it was impregnated with CTD 1202x liquid ceramic binder and cured. The outer layer was wound on top of the cured inner layer, after covering it with preformed ceramic interlayer insulation made of 3 layers of 0.125 mm ceramic sheets. The outer layer is also impregnated with binder and the double-layer coil is cured again to set the size for reaction. Curing is done at 150^{o}C for 30 min in a closed cavity mold.

Coil reaction is done in a closed fixture set to the nominal coil size. The target reaction cycle consisted of three ramps, followed by three temperature plateaus. Table II shows the actual parameters of the heat treatment cycle as read by thermocouples mounted within the oven. Coil radial ground insulation consisted of 3 layers of 0.125 mm ceramic sheet. A quench protection heater, consisting of 2 stainless strips bonded to a 0.100 mm thick piece of Kapton, was placed between the outer coil and the first sheet from the outer coil surface in each quadrant. Flexible NbTi leads were soldered at the parting plane to each of the inner and outer Nb_3Sn lead using 70%Pb-30%Sn solder.

Voltage taps were soldered across each coil block to detect and localize quenches. Coils were impregnated with CTD101K epoxy, in the same fixture that was used for reaction, and cured at 125^{o}C for 21 hours. The coil dimensions were measured after impregnation in the free state to select appropriate pre-stress shims.

TABLE II. Coil Heat Treatment Cycle.

Step	Time, h	Coil Ave. T, °C	Witness Ave. T, °C
RT to 205°C	90		
205- 215°C	80	211± 3	212± 1
215°C to 390°C	7		
390- 410°C	47	403± 7	405± 3
410°C to 640°C	7.5		
640-650°C	52	645± 7	646± 4

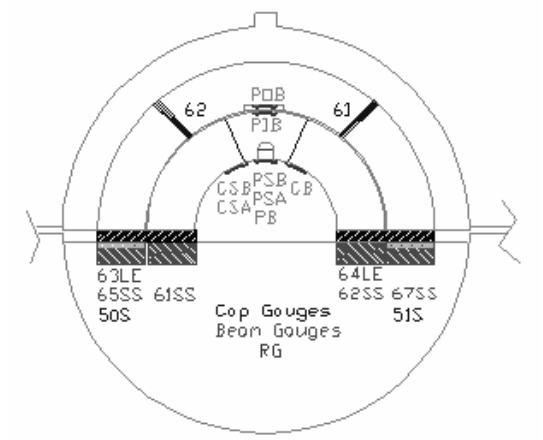

FIGURE 5. Gauge positions with respect to coil.

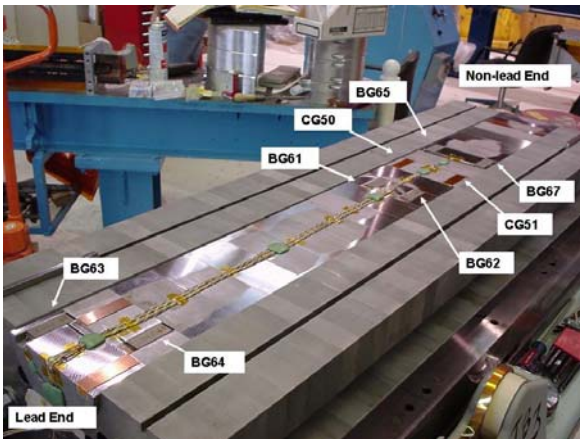

FIGURE 6. Coil midplane instrumentation.

MIRROR DESIGN, INSTRUMENTATION AND ASSEMBLY

To reduce the fabrication cost and turnaround time for coil testing, a mirror configuration was used [9]. The cross-section of the mirror mechanical structure is shown in Figure 4. This structure is similar to the dipole structure except that the iron yoke is split horizontally and one of the two half-coils in the magnetic mirror configuration is replaced by half-cylinder blocks made of solid iron. Aluminum-bronze spacers surround the coil inside the yoke. Stainless steel shims between the mirror and coil midplane and radial Kapton shims between the coil, spacers and yoke are used to control the coil prestress. Transverse coil preload is applied by a combination of the aluminum yoke clamps and thick bolted stainless steel skin. Axial preload is applied through end preload bolts attached to the thick end plates.

The magnet assembly started with installation of iron mirror blocks into the lower yoke. The coil was then placed onto the mirror, the upper yoke blocks installed, and the yoke clamps inserted. Skin halves were placed around the yoked assembly and bolted together. Bolting was done in several steps, while stress in the coil and end spacers was monitored by the gauges. After the skins were installed, 50 mm thick end plates were bolted to the skin ends.

To control the coil azimuthal preload, both capacitive and resistive strain gauges were used. The general position of the gauges with respect to the coil cross section is shown in Figure 5. Capacitive gauges (designated CG) and beam gauges (designated BG) were imbedded into the mirror at the midplane as shown in Figure 6. Gauges BG63 and BG64 measured preload at the inner and outer splices, respectively. Gauges BG61 and BG62 measured inner coil body preload. Gauges BG65, BG67, CG50 and CG51, measured outer coil body preload. In addition to the midplane gauges, two capacitive gauges, CG62 and CG61, were placed at the outer pole in the body, at the same longitudinal position as gauges CG50 and CG51, with CG62 opposing CG50 and CG61 opposing CG51, as shown in Figure 5. In the body, resistive strain gauges were glued to the inside surface of the impregnated coil (CB, CSA and CSB). Resistive gauges were also mounted on the inner surfaces of inner and outer pole blocks (PIB and POB), on the aluminum bronze spacers, and on the skin near the magnet center. The axial coil preload was controlled through the resistive gauges on the bolts.

To determine the coil target prestress, ANSYS analysis was performed with elastic and plastic (more realistic) coil properties. In the first case the target coil prestress was 125 MPa

TABLE III. HFDM06 coil prestress.

Gauges	Measurements, MPa	FEA-elastic, MPa	FEA-plastic, MPa
BG61,62	50	15	20
BG65,67	50	60	50
CG61,62	50	30	40
CB, CSA, CSB	25-50	100	50

for the inner-layer pole turn and 100 MPa for the outer-layer pole turn. In the second case the maximum coil prestress values for the same assembly shims are smaller (90 MPa and 70 MPa respectively). Table III summarizes the results of coil prestress measurements by the coil gauges and calculations for the gauge location. There is a good correlation of measurements with plastic calculations. The measurement data confirm that the target coil prestress during assembly has been achieved.

TEST RESULTS

HFDM06 was tested in boiling liquid He at both 4.5 K and lower temperatures. The quench history of HFDM06 is shown in Figure 7. Magnet training started at a helium bath temperature of 4.5 K with a nominal current ramp rate of 20 A/s. The first training quench was at 15.2 kA. Then, after a period of relatively rapid increase, the magnet training rate slowed down, establishing an erratic "plateau" at the current level of 22 kA, well below the expected magnet short sample limit. During the ramp rate studies performed later, the magnet training process was continued, raising the maximum quench current to 23.5 kA. To accelerate the training, the magnet was cooled down to 2.2 K and quenched several times. The maximum quench current at this temperature was distributed over a larger current range of 20.4-23.4 kA, and were lower than the maximum quench current reached during the ramp rate measurements at 4.5 K. Magnet quenching at the higher temperature of 3.5 K led to higher currents of ~24.3 kA, indicating that the magnet training process was not complete.

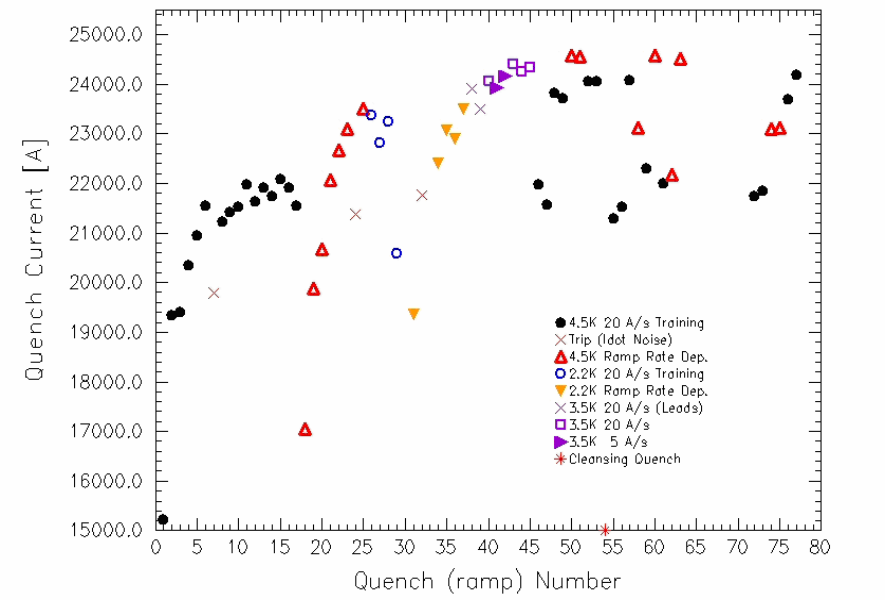

Figure 7. HFDM06 quench history.

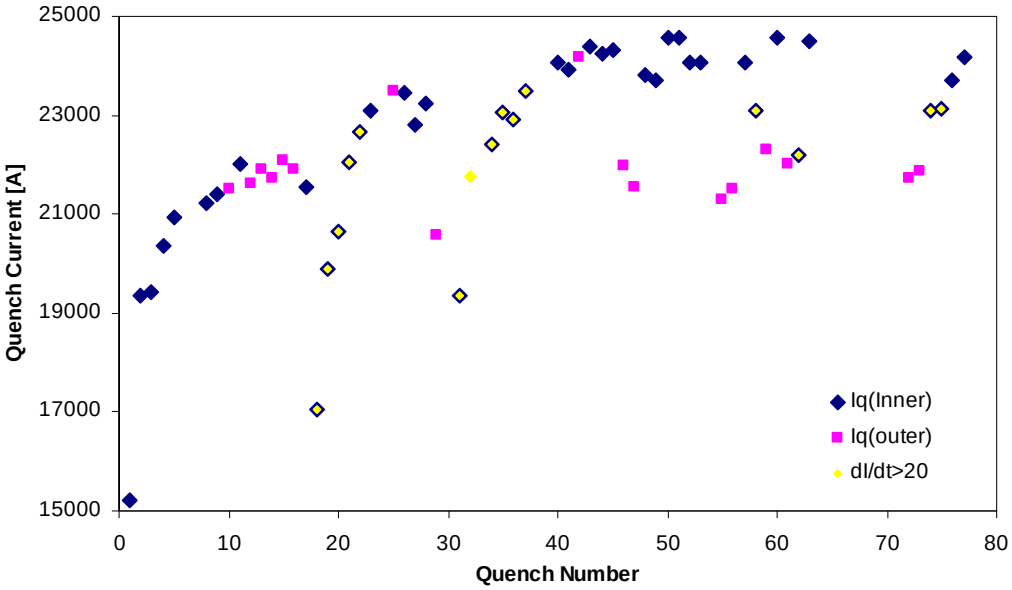

Figure 8. Quench origin during magnet training. High ramp rate quenches are separately identified.

When warmed up to 4.5 K again, the magnet demonstrated erratic quench performance with quench currents spread within the range between 21 and 24 kA. The maximum quench current of 24.56 kA reached at 4.5 K corresponds to the maximum field in the coil of 11.43 T.

Some system trips occurred during the magnet test, were caused in part by low quench detection threshold settings. At 3.5 K, two quenches in the superconducting leads occurred above 23 kA due to low LHe level. These events are indicated in Figure 7 by the cross marks.

The quench location and development time for training quenches are shown in Figures 8 and 9. As can be seen, the quench currents, their locations and timing are correlated: quenches either in the outer layer or at lower current in the inner layer generally develop more slowly.

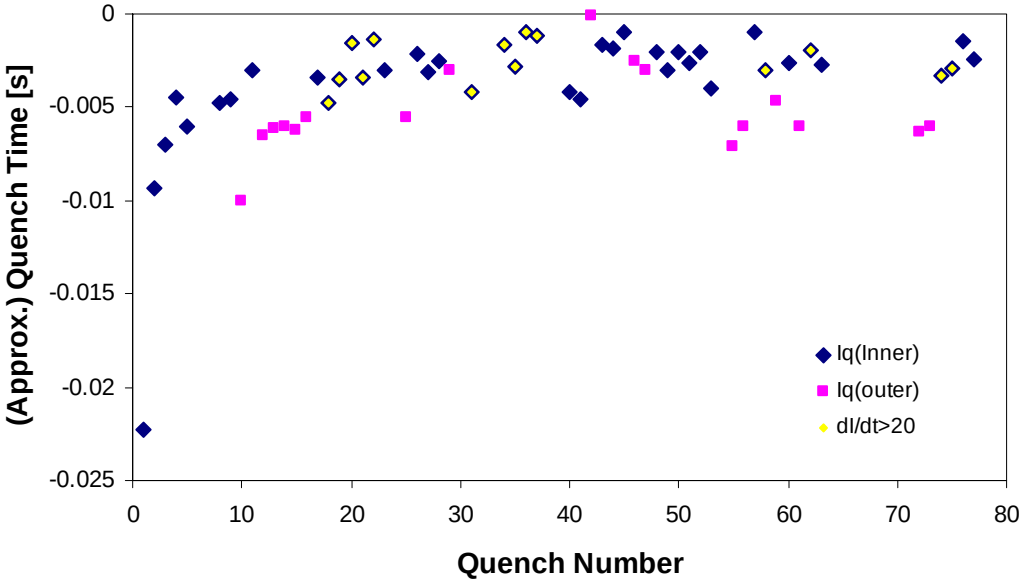

Figure 9. Quench development time for inner and outer layer training quenches. High ramp rate quenches are separately identified.

Data in Figure 8 show that most of the outer layer quenches occurred at currents between 21 and 22 kA. Based on the data from strain gauges, the outer-layer was under compression at all currents. Thus, taking into account the random occurrence of the outer layer quenches during training, these quenches could be attributed to the flux jump instabilities in the outer layer turns [10].

The Voltage Spike Detection System (VSDS) [11] captured spike data for all current ramps at a threshold of from 15 to 17 mV. There were fewer spikes in HFDM06 than in the previously tested two mirror models HFDM04 and HFDM05, which were made of the first generation RRP strand with similar sub-element size [12]. The level of current density at which the flux jump quenches occurred was also 30% higher in HFDM06 than in the previously tested mirror models. This difference is likely due to the higher value of copper matrix RRR in the HFDM06 and the lower level of sub-element deformation and merging in the cable used in this model. Based on measurements, the cable RRR in all HFDM06 coil segments was consistent with the value of 172±3. These numbers are in good agreement with measurements on strand samples and the small racetrack coil made of the same cable [4]. However, they are about an order of magnitude higher than in HFDM04-05.

The ramp rate sensitivity of magnet quench current at 4.5 and 2.2 K is shown in Figure 10. The ramp rate studies show that at 4.5 K the magnet short sample limit was reached at all current ramp rates. At 2.2 K the magnet short sample limit was reached at current ramp rates above 200 A/s. At lower ramp rates the magnet was limited by mechanical (incomplete training) or electromagnetic (flux jumps) instabilities.

Round and extracted strands were included as witnesses during coil reaction to evaluate the coil short sample limits (SSL). Based on witness sample test data the SSL calculated at 4.5 K was 24.5-25.5 kA. From Figure 19, the coil maximum quench current at 4.5 K extrapolated to 0 A/s is about 24.8 kA. The calculated range of SSL at 4.5 K is in good agreement with the magnet test results. The values of witness sample RRR were within 157±17, which is also in good agreement with the HFDM06 coil.

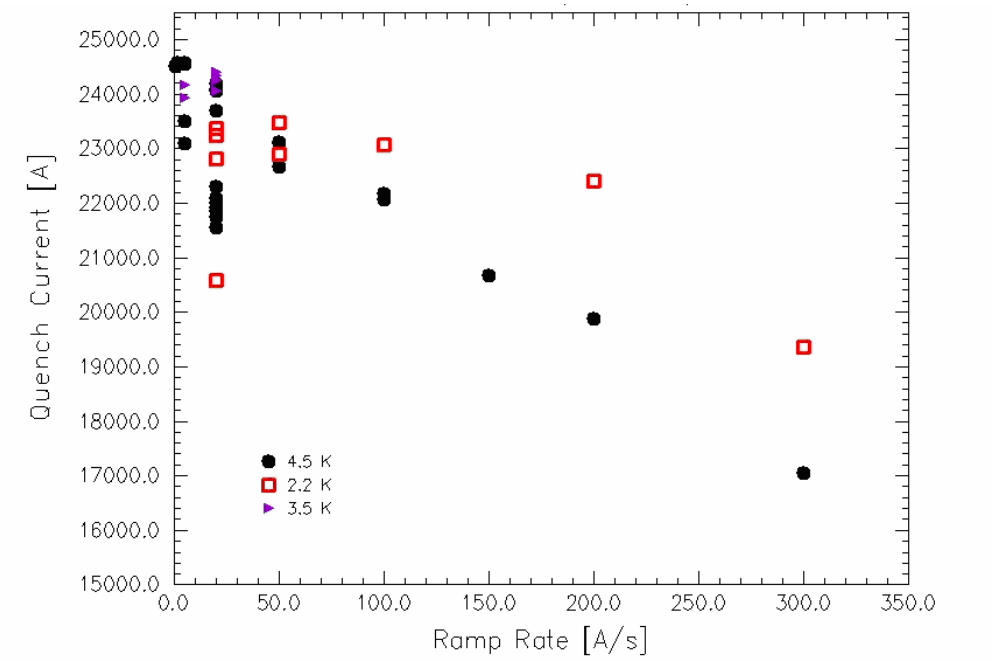

Figure 10. HFDM06 quench current vs current ramp rate at various temperatures.

CONCLUSIONS

The 108/127 stack Nb_3Sn RRP strand has been developed by OST and tested at Fermilab. The reduction of sub-element size in the 1 mm strand to ~70 microns in combination with general RRP technology optimization resulted in improved flux jump stability of this conductor, preserving its high level of critical current density and RRR. Rutherford cables made of 1-mm strand demonstrated good stability and low degradation of major parameters. The first 1-m long two-layer cos-theta coil made of the 27-strand cable reached its short sample limits at 4.5 K, producing a field above 11 T. The second coil made of the same cable will be tested soon. In spite of the high RRR value provided in the new strand and preserved during cable and coil fabrication, flux jump instabilities in the superconductor were still observed and affected magnet quench performance. The work on the optimization of this strand design will continue.

ACKNOWLEDGEMENTS

This work is supported by the U.S. Department of Energy. The authors thank technical staff of Fermilab's Technical Division for their contributions to magnet fabrication and test.

REFERENCES

1. A.V. Zlobin et al., **"**R&D of Nb_3Sn Accelerator Magnets at Fermilab", IEEE Transactions on Applied Superconductivity, Vol. 15, Issue 2, June 2005 Page(s): 1113-1118.
2. A.V. Zlobin et al., "Nb_3Sn Accelerator Magnet Technology R&D at Fermilab", Proceedings of 2007 Particle Accelerator Conference, Albuquerque, NM, June 2007.
3. J.A. Parrell et al., "Advances in Nb_3Sn strand for fusion and particle accelerator applications", IEEE Transactions on Applied Superconductivity, Vol. 15, Issue 2, 2005, p. 1200.
4. E. Barzi et al., "Performance of Nb_3Sn RRP strands and cables based on a 108/127 Stack Design", IEEE Transactions on Applied Superconductivity, Vol. 17, Issue 2, June 2007 Page(s): 2718-2721.
5. S. Hong et al., "Latest Improvements of Current Carrying Capability of Niobium Tin and Its Magnet Applications", IEEE Transactions on Applied Superconductivity, Vol. 16, Issue 2, 2005, p. 1146.
6. N. Andreev et al., "Development of Rutherford-type Cables for High Field Accelerator Magnets at Fermilab", IEEE Transactions on Applied Superconductivity, Vol. 17, Issue 2, June 2007 Page(s): 1027-1030.
7. G. Ambrosio et al., "Development of the 11 T Nb_3Sn Dipole Model at Fermilab", IEEE Transactions on Applied Superconductivity, Vol. 10, Issue 1, March 2000, p.298.
8. D.R. Chichili et al., "Fabrication of the Shell-Type Nb_3Sn Dipole Model at Fermilab", IEEE Transactions on Applied Superconductivity, Vol. 11, Issue 1, March 2001, p. 2160.
9. D.R. Chichili et al., "Design, Fabrication and Testing of Nb_3Sn Shell Type Coils in Mirror Magnet Configuration", CEC/ICMC 2003, Alaska, September 22-25, 2003.
10. A.V. Zlobin, V.V. Kashikhin, E. Barzi, "Effect of Magnetic Instabilities in Superconductor on Nb_3Sn Accelerator Magnet Performance", IEEE Transactions on Applied Superconductivity, Vol. 16, Issue 2, June 2006 Page(s): 1308-1311
11. D. F. Orris, et al., "Voltage Spike Detection in High Field Superconducting Accelerator Magnets", IEEE Transactions on Applied Superconductivity, Vol 15, Issue 2, 2005, p. 1205.
12. R. Bossert et al., **"**Development and Test of Nb_3Sn Cos-Theta Coils Made of High-J_c RRP Strands", CEC/ICMC 2005, Colorado, August-September 2005.